PCCP

PAPER

View Article Online
View Journal | View Issue

Cite this: *Phys. Chem. Chem. Phys.*, 2017, **19**, 22049

Triplet–triplet annihilation upconversion kinetics of C_{60}–Bodipy dyads as organic triplet photosensitizers†

Yaxiong Wei,[a] Miaomiao Zhou,[bc] Qiaohui Zhou,[a] Xiaoguo Zhou,*[ad] Shilin Liu,[ad] Song Zhang*[bc] and Bing Zhang[bc]

Received 8th June 2017,
Accepted 1st August 2017

DOI: 10.1039/c7cp03840b

rsc.li/pccp

Three new triplet photosensitizers consisting of a bodipy derivative and C_{60} moieties were synthesized for triplet–triplet annihilation upconversion of perylene. With the extension of the π-conjugated structure of the bodipy derivative, the three photosensitizers exhibited different absorption wavelengths, *e.g.* 517 nm for **B-2**, 532 nm for **B-4**, and 557 nm for **B-6**. The steady-state and transient absorption, steady-state fluorescence, and upconverted fluorescence emission were investigated to reveal step-by-step the dynamic processes of the above systems. The quantum yields of intramolecular energy transfer, intersystem crossing, and triplet–triplet energy transfer were measured. From the upconverted fluorescence emission spectra, the overall quantum yield of the triplet–triplet annihilation upconversion, Φ_{UC}, was determined to be 5.80% for **B-2**, 7.95% for **B-4**, and 4.99% for **B-6**.

1. Introduction

Triplet photosensitizers are widely used in many fields, such as photocatalysis of organic reactions,[1–4] photodynamic therapy (PDT),[5–8] photovoltaics,[9,10] luminescent molecular probes,[11] and triplet–triplet annihilation (TTA) upconversion.[12–15] In a common TTA upconversion (TTA-UC) system, the excited energy is first transferred from a triplet photosensitizer to an acceptor, and then the acceptor molecule in the singlet excited state can be produced *via* Dexter energy transfer of two triplet acceptors with a high upconversion quantum yield.[14,16,17] Most triplet photosensitizers for the TTA upconversion are the transition-metal complexes, such as polyimine Ru(II), cyclometalated Ir(III), and Pt(II)/Pd(II) porphyrin complexes.[18–20] In these photosensitizers, the transition-metal atom effect facilitates intersystem crossing (ISC) of a photosensitizer to produce its triplet state after photoexcitation.[21,22] However, these complexes are expensive and usually have relatively weak absorption in the visible wavelength range.[5,23,24] A type of metal-free triplet sensitizer in TTA-UC is bromo- or iodo-Bodipy, which is extensively applied to sensitize singlet oxygen ($^1O_2$).[13,25,26] The most important advantage of these photosensitizers is the strong absorption in the visible range. All the above triplet photosensitizers require the heavy atom effect, like Pt(II), Ir(III), bromine, iodine, *etc.* It is difficult to effectively prepare the triplet state of organic chromophores with a lack of heavy atoms.[8,27] There are only a few organic photosensitizers without any heavy atoms reported, *e.g.* benzophenone, 2,3-butanedione, *etc.*[28–30] Therefore, it would be very important to develop a series of organic triplet photosensitizers which have a general molecular structure for being heavy-atom-free with a high ISC efficiency. For this, there is still a long road ahead and it is full of challenges.

Since it was discovered in 1985,[31] C_{60} has attracted a lot of concern. Molecular orbital calculations show that C_{60} has a large delocalization energy and exhibits some remarkable chemical features, especially a high ISC efficiency close to unity.[32] However, the very weak absorption of C_{60} in the visible region (400–650 nm) makes it unsuitable as an ideal photosensitizer.[33] Thus, resonance energy transfer (RET) from a light-harvesting antenna to C_{60} becomes a potential method to excite C_{60}.[34–37] Furthermore, the bridging connection between the C_{60} unit and an antenna is proposed to produce a general molecular structure of an organic triplet photosensitizer, which certainly generates some outstanding physicochemical properties in supramolecular photochemistry.[38,39] After photoexcitation of the antenna, the triplet state of C_{60} is finally populated *via* the intramolecular

[a] *Hefei National Laboratory for Physical Sciences at the Microscale and Department of Chemical Physics, University of Science and Technology of China, Hefei, Anhui 230026, China. E-mail: xzhou@ustc.edu.cn*
[b] *State Key Laboratory of Magnetic Resonance and Atomic and Molecular Physics, Wuhan Institute of Physics and Mathematics, Chinese Academy of Sciences, Wuhan 430071, China. E-mail: zhangsong@wipm.ac.cn*
[c] *University of Chinese Academy of Sciences, Beijing 100049, China*
[d] *Synergetic Innovation Center of Quantum Information & Quantum Physics, University of Science and Technology of China, Hefei, Anhui 230026, China*

† Electronic supplementary information (ESI) available: Synthetic processes of major compounds; NMR and HR-MS spectra; femtosecond transient difference absorption spectra; TTA-UC spectra. See DOI: 10.1039/c7cp03840b

RET from the antenna to the C_{60} unit followed by ISC of the C_{60} moiety.

Several C_{60}–organic chromophore dyads or triads have been designed and synthesized with strong visible absorption. The application of these dyads or triads in photocatalysis of organic reaction or photodynamic therapy (PDT) has been reported.[36,40–42] Due to its strong visible absorption and the versatile derivatization of its chemistry, bodipy and its derivatives have been generally used for photosensitizers as the light-harvesting antenna.[5,43–46] Recently, dyads based on bodipy and C_{60} unities as the triplet photosensitizers for TTA upconversion have been investigated.[47,48] The overall TTA-UC quantum yields of three dyads with perylene were measured to be 2.9% for carbazole–bodipy–carbazole–C_{60} dyad, 2.9% for bodipy–thiophene–C_{60}, and 7.0% for bodipy–bodipy–benzene–C_{60} triad. However, the details of the kinetic process of these TTA-UC systems are still unclear, *e.g.* the RET rate, the quantum efficiencies of triplet–triplet energy transfer from the dyads to perylene, the dependence of the energy transfer rate on molecular geometries, the dependence of the upconversion quantum yield on the excitation power density, and so on. Additionally, the concentration effect was investigated recently in triplet state absorption–emission of a fullerene-functionalized Pt(II) metallacycle.[49]

In this work, three triplet photosensitizers of C_{60}–Bodipy dyads were synthesized and composed new TTA upconversion systems with perylene, where bodipy acted as the light-harvester in the visible wavelength range, and C_{60} was the energy acceptor to convert the electron spin. With the extension of the π-conjugated structure of the bodipy derivative, the three photosensitizers exhibit different absorption wavelengths. The steady-state absorption and fluorescence emission, transient absorption, and TTA-UC fluorescence emission have been measured to reveal step-by-step the dynamic processes of the above systems, including the intramolecular RET, ISC of the dyads, and quantum yield of TTA-UC. Based on the measured dynamic information, an overall kinetic description is proposed for the TTA-UC system of C_{60}–bodipy dyads.

2. Experimental section

2.1 Synthesis and characterization

All the precursors of analytical reagents were purchased from Sigma-Aldrich Co. without any purification. Solvents were dried and distilled prior to synthesis. The purified toluene was used as the solvent in the following spectral and dynamic experiments. The overall synthetic processes of the three C_{60}–bodipy dyads are summarized in Scheme 1.

Compounds **1–6** were prepared by following the synthetic methods in ref. 48 for **1–3** and ref. 47 for **4–6**. The Suzuki and Sonogashira coupling reaction catalyzed by Pd(0) was used to connect bodipy and phenylboronic acid (or 4-formylphenylboronic acid) in **B-1**, **B-3**, and **B-5**, and compound **7**, **10** and **11**, respectively. The Prato reaction of compound **7**, **10**, and **11** and sarcosine with C_{60} produced the C_{60}–bodipy dyads of **B-2**, **B-4**, and **B-6**. All the compounds were synthesized with a good yield. The molecular structures of the compounds were verified by ^{1}H NMR spectroscopy and high-resolution mass spectrometry. The details of the synthetic processes and the above spectra are summarized in the ESI.†

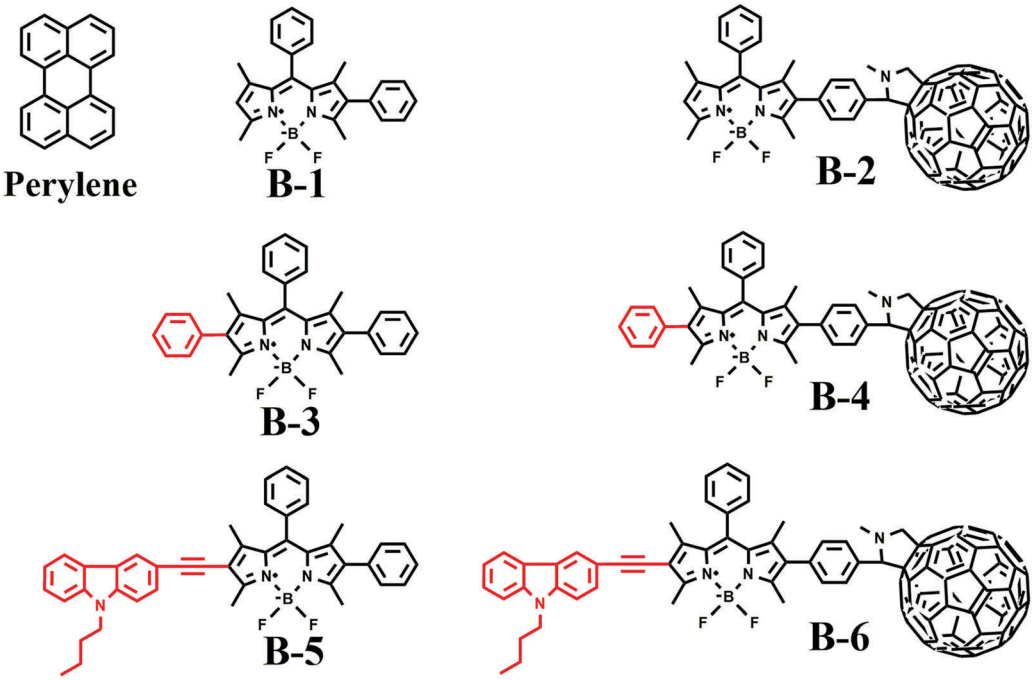

Scheme 1 Structures of the triplet photosensitizers **B-2**, **B-4**, and **B-6** and the light antenna of **B-1**, **B-3**, and **B-5**, as well as the triplet acceptor perylene.

2.2 Experimental equipment

^{1}H NMR spectra were recorded using a 400 MHz spectrophotometer (AVANCE III 400, Bruker), where $CDCl_3$ was used as the solvent and TMS was the standard for which δ = 0.00 ppm. High-resolution mass spectra were measured using a spectrometer (GCT, Micromass UK). The photochemical behaviors of the chemicals were investigated using the steady-state and transient absorption spectra. UV-Vis absorption spectra were recorded in a wavelength range of 300–800 nm using a spectrophotometer (UV-3600, Shimadzu). The steady-state fluorescence emission was measured using a fluorescence spectrophotometer (F-4600, Shimadzu), within a wavelength range of 400–800 nm.

The femtosecond and nanosecond time-resolved transient absorption spectra were used to investigate the photochemical behaviors of the compounds. The details of the femtosecond transient absorption spectrometer have been described elsewhere,[50] and thus only a brief introduction is given here. A 800 nm femtosecond laser with 35 fs pulse width was generated by a Ti:sapphire pumped by the CW second harmonic of a Nd:YVO4 laser and amplified by a Nd:YLF laser, with a maximum energy of 1 mJ per pulse. A 400 nm pulse with an energy of 100 μJ was yielded from a frequency double of a 1 mm thick BBO crystal and used to pump NOPA. The output NOPA was used as the excitation pulse at 532 nm in the present experiment. The energy was attenuated to about 4.5 μJ. A fraction of the 800 nm laser was focused on a CaF_2 plate to produce a white light continuum. The white light reflected from the front and back surfaces of the quartz plate were used as the probe and reference beams. The relative polarization of the pump and probe pulses was maintained as 54.7°. The absorption spectra were detected with a CCD camera equipped with a spectrometer (Princeton, SpectraPro 2500i). The instrumental response function was better than 150 fs.

Nanosecond time-resolved transient absorption spectra were measured with a home-built laser flash photolysis system. The second harmonic (532 nm) of a Q-Switched Nd:YAG laser (PRO-190, Spectra Physics) was used as the excitation source (pulse duration 8 ns, repetition rate of 10 Hz, pulse energy $<$10 mJ per pulse). A 500 W Xenon lamp was used as the analyzing light, and passed through a flow quartz cuvette perpendicular to the pulsed laser. The optical absorption path length was 10 mm. A monochromator equipped with a photomultiplier (CR131, Hamamatsu) was used to record the transient absorption spectra within a wavelength range of 320–700 nm. The typical spectral resolution was less than 1 nm. A dynamic decay curve of the intermediate was averaged by multi-shots and recorded with an oscilloscope (TDS3052B, Tektronix). All the solutions were deoxygenated by purging with high purity argon (99.99%) for about 20 minutes prior to measurements.

A diode pumped solid-state CW laser (532 nm) was used as the excitation light source in the upconversion experiment. The diameter of the laser spot is ~3 mm. In the TTA-UC experiment, the solution of photosensitizers and perylene was deoxygenated by purging with high-purity argon for at least 20 minutes, and the gas flow was kept during the TTA-UC measurement. With photoexcitation at 532 nm, the upconverted fluorescence of perylene was measured with a modified commercial spectrometer. The fluorescence was dispersed and detected with a triple monochromator system (TriplePro, Acton Research) and a CR131 photomultiplier. The normal spectral resolution was ~1.0 nm.

2.3 Theoretical calculations

The geometries of the compounds were optimized using density functional theory (DFT) with the B3LYP function and 6-31G(d) basis set. No imaginary frequencies were found for all optimized structures. The spin density surfaces of the dyads were calculated at the same level of theory. The energy gaps between the ground state and the triplet excited states were calculated, and the vertical excitation energies were used to compare with the experimental data in the absorption spectra. The PCM model was applied to evaluate the solvent effect. All these calculations were performed using the Gaussian 09W program package.[51]

3. Results and discussion

3.1 Steady-state UV-Vis absorption and fluorescence spectra

The steady-state UV-Vis absorption spectra of C_{60}, light-harvesting antenna (**B-1**, **B-3**, **B-5**), and photosensitizers (**B-2**, **B-4**, **B-6**) were recorded and shown in Fig. 1(a). Both the antenna **B-1** and photosensitizer **B-2** have a strong absorption at 517 nm, and the

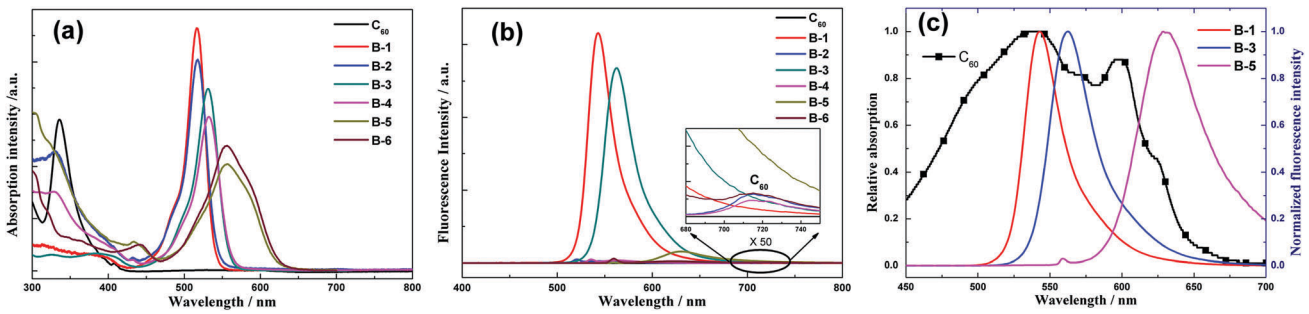

Fig. 1 (a) UV-Vis absorption spectra of C_{60}, the C_{60}–bodipy dyads (**B-2**, **B-4**, and **B-6**) and the light-absorbing antennas (**B-1**, **B-3** and **B-5**). (b) Fluorescence emission spectra of C_{60} (λ_{ex} = 532 nm), **B-1**, **B-2** (λ_{ex} = 517 nm), **B-3**, **B-4** (λ_{ex} = 532 nm), **B-5** and **B-6** (λ_{ex} = 556 nm). (c) Normalized UV-Vis absorption spectra of C_{60} in 450–700 nm and the normalized fluorescence emission spectra of **B-1**, **B-2**, and **B-3** (in toluene, $c = 1 \times 10^{-5}$ M, 25 °C).

corresponding molar extinction coefficients ε are 93 000 M^{-1} cm^{-1} for **B-1** and 81 000 M^{-1} cm^{-1} for **B-2**. Although the **B-1** core is connected to a C_{60} moiety, the absorption of **B-2** does not show an apparent wavelength-shift from that of **B-1**, implying that the vertical excitation energy of the singlet state S_1 of **B-2** is kept as it is in the **B-1** core. Moreover, the intensities of the absorption bands of **B-2** are changed a bit from those of **B-1** and C_{60}. Thus, weak electronic interactions exist between **B-1** and the C_{60} moieties in **B-2**, and certainly they are not strong enough to change the energies of the main molecular orbits and spin density surface. Our theoretical calculations have also confirmed the conclusion. Similar phenomena were observed in the absorption spectra of **B-3** and **B-5**, and **B-4** and **B-6**. Moreover, the absorption band in the visible range shows a remarkable red-shift with the extension of the π-conjugated structure of the bodipy derivative, *e.g.* 532 nm for **B-3** and 556 nm for **B-5**. Meanwhile, the band is apparently broadened, and the maximal value of ε is decreased. All three C_{60}–bodipy dyads, **B-2**, **B-4** and **B-6**, have similar strong absorption bands in the visible range of 500–600 nm to the antennas, **B-1**, **B-3** and **B-5**, and thus they are also good solar light-harvesting antennas and used in triplet photosensitizers in the present experiments. Different from the antennas and dyads, C_{60} has a very weak absorption in the visible range of 450–650 nm. Thus, the direct photoexcitation of C_{60} with a visible photon is of low efficiency, and C_{60} is not a satisfactory light-harvestor.[33,35,37]

Fig. 1(b) shows the fluorescence emission spectra of the C_{60}, antennas, and dyads. The three antennas, **B-1** **B-3** and **B-5**, have strong emission at 543 nm (Φ_F = 82.3% for **B-1**), 561 nm (Φ_F = 68.3% for **B-3**), and 629 nm (Φ_F = 11.0% for **B-5**), respectively. On the contrary, the fluorescence of the dyads, **B-2**, **B-4** and **B-6**, is almost completely quenched, and only very weak emission can be detected at 543 nm (Φ_F = 0.4% for **B-2**), 562 nm (Φ_F = 0.1% for **B-4**), and 624 nm (Φ_F = 0.1% for **B-6**). Therefore, the intramolecular energy transfer between the excited antennas and C_{60} in the dyads is very efficient.

Usually, resonance energy transfer (RET) becomes efficient when the emission band of a donor overlaps with the absorption of an acceptor. The more serious the overlap is, the faster RET occurs. As shown in Fig. 1(c), the emission spectra of **B-1** and **B-3** almost completely overlap with the absorption band of C_{60}, while the overlap between **B-5** and C_{60} is relatively low. Therefore, intramolecular RET in the three C_{60}–bodipy dyads is expected with a high efficiency, and the efficiencies of **B-2** and **B-4** are higher than that of **B-6**. As listed in Table 1, the RET efficiencies of **B-2**, **B-4**, and **B-6** are determined in the experiment as 99.5%, 99.9%, and 99.1%, respectively.

3.2 Femtosecond transient difference absorption spectra and DFT calculations

In order to reveal the initial photophysical process of the photosensitizers under irradiation, the femtosecond transient absorption spectra of **B-2**, **B-4**, and **B-6** in toluene were measured under excitation at 532 nm, and are shown in Fig. 2. In addition to a very strong stimulated emission or ground-state bleaching band (negative peak), several specific positive peaks are observed notably, especially in the wavelength range of 330–470 nm.

Table 1 Photophysical characteristics of C_{60}, the antennas (**B-1**, **B-3**, and **B-5**) and the C_{60}–Bodipy dyads (**B-2**, **B-4**, and **B-6**) in toluene at 25 °C

Compound	λ_{abs}	λ_{em}	ε^a	$\Phi_F{}^b$ (%)	$\Phi_{ET}{}^c$ (%)
C_{60}	283/336/532	415/439/680	4.7/5.8/0.04	—	—
B-1	517	543	9.3	82.3 ± 2.0	—
B-2	518	543	8.1	0.4 ± 0.1	99.5 ± 0.1
B-3	531	561	7.0	68.3 ± 2.0	—
B-4	532	562	5.9	0.10 ± 0.02	99.9 ± 0.1
B-5	556	629	4.8	11.0 ± 1.0	—
B-6	557	624	4.1	0.10 ± 0.02	99.1 ± 0.1

[a] Molar extinction coefficient ε is obtained at the optimal absorption wavelength, and the unit is 10^4 M^{-1} cm^{-1}. [b] Fluorescence quantum yields are calculated using compound **3** as a standard, $\Phi_F(\mathbf{3})$ = 2.7% in ACN. [c] ET efficiency is calculated as $\Phi_{ET} = 1 - \Phi_{da}/\Phi_d$.

Taking the spectra of **B-4** in Fig. 2(b) as an example, positive bands that appeared at 352 and 429 nm were observed and assigned to the excited state absorption (ESA). Both the peaks reached the maximum within ~300 fs and then were quickly attenuated during the first 1 ps. Thus, they were attributed to the $S_n \leftarrow S_1$ absorption, and the decay processes occur *via* nonradiative transition. Afterwards, a new peak at 375 nm was produced, and its intensity was kept unchanged up to the longest delay time we measured. Naturally, the band of long lifetime is attributed to the absorption of the triplet state, $T_n \leftarrow T_1$. The corresponding resonance wavelength agrees with the characteristic absorption of $^3C_{60}$*.[34] Therefore, an ISC process is expected to produce the triplet state T_1, and the triplet state is located in the C_{60} unit. In addition, the dynamic behavior of the wide peak at 725 nm is a bit strange. It is quickly decreased in 1 ps after reaching the maximum, and then retains its intensity for a long time as noticed in Fig. 2(b). According to this, another characteristic absorption of $^3C_{60}$* was located at ~716 nm,[34] and the absorption of the $^3C_{60}$* moiety is naturally slightly shifted in the C_{60}–bodipy dyads. Therefore, the band at 725 nm is attributed to the overlap between the absorption of $^3C_{60}$* and ESA. The overlap disappears in the absorption spectra of **B-2** and **B-6**, as the ESAs are located at 782 nm for **B-2** and 785 nm for **B-6** as shown in Fig. 2(a) and (c), respectively.

As shown in Fig. 2, the other spectra of the dyads of **B-2** and **B-6** are similar to those of **B-4**. For **B-2** in Fig. 2(a), the positive bands centered at 352, 433, and 782 nm are attributed to the $S_n \leftarrow S_1$ absorption, while the bands at 370 and 735 nm correspond to the transition between the triplet states, respectively. Simultaneously, for **B-6** in Fig. 2(c), the absorptions at 345, 470, and 785 nm are attributed to the ESA of the S_1 state, while the 368 and 726 nm peaks are the absorptions of the triplet state.

From the spectra, the lifetimes of the singlet excited state S_1 can be derived as well as the ISC rate from the S_1 to T_1 state. The best dynamic parameters in the initial decay process of **B-2**, **B-4** and **B-6** were obtained by the least square fitting and listed in Table 2. Based on the naturally physical mechanisms,

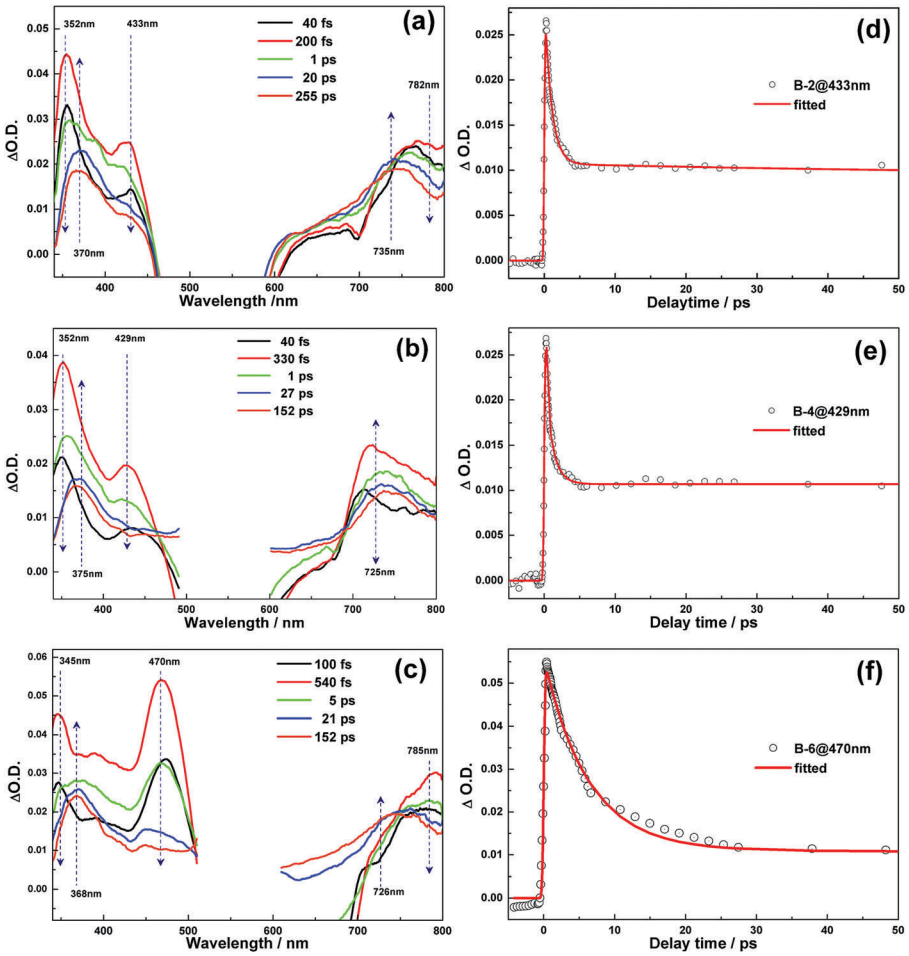

Fig. 2 Femtosecond transient difference absorption spectra of **B-2** (a), **B-4** (b), and **B-6** (c), and the experimental (dotted lines) and fitted (solid lines) decay curves of the absorption band for **B-2** at 433 nm (d), **B-4** at 429 nm (e), and **B-6** at 470 nm (f) in toluene (25 °C), under excitation at 532 nm.

a tri-exponential kinetic model was applied to fit the absorption curves at the typical wavelength of 433 nm for **B-2**, 429 nm for **B-4** and 470 nm for **B-6**, respectively, shown in Fig. 2(d–f). As suggested by the steady-state absorption spectra in Fig. 1(a), the bodipy core is initially excited to the S_1 excited state under excitation at 532 nm. Then its decay process involves the competing processes of fluorescence emission, internal conversion, and singlet attenuation energy transfer from the bodipy core to the C_{60} moiety.

To evaluate the contributions of fluorescence emission and internal conversion, the femtosecond transient absorption spectra of **B-1**, **B-3**, and **B-5** were measured and their dynamic processes were fitted respectively (Fig. S9–S14 of the ESI†). The natural decay rate constants are 2.97×10^8 s^{-1} for **B-1**, 3.72×10^8 s^{-1} for **B-3**, and 8.43×10^8 s^{-1} for **B-5**, which are listed in Table 2 and consistent with the lifetimes of bodipy derivatives reported in the previous experiments.[48,52,53] Therefore, the rates of internal conversion of the dyads should be around 10^8 s^{-1} similar to those of the antennas, and the observed fastest attenuation with a rate of $1/\tau_1$ ($\sim 10^{11}$ s^{-1}) in the dyads must proceed along with RET from the bodipy core to the C_{60} moiety as in eqn (1). The product, $^1C_{60}$*–bodipy, can further transform into its triplet state T_1, $^3C_{60}$*–bodipy, *via* a fast ISC process as in eqn (2), according to the high ISC quantum efficiency (Φ_{ISC} = 1.0) of the C_{60} unit. The corresponding characteristic time is noticed as τ_2 in the kinetic model. From the produced triplet state T_1, the third decay process with a rate of $1/\tau_3$ involves other slow processes like collision. Here we pay more attention to the energy transfer rate to yield $^1C_{60}$* and the ISC process of the C_{60} unit, and thus Table 2 only summarized the obtained rates $1/\tau_1$ and $1/\tau_2$. For the singlet RET from the bodipy core to C_{60}, $1/\tau_1$ in **B-2** and **B-4** are much faster than that in **B-6**. This agrees very well with the aforementioned conclusions of UV-visible absorption and emission spectra, where the emissions of **B-2** and **B-4** completely

Table 2 The decay rates of **B-2**, **B-4**, **B-6** in toluene at room temperature

Compound	$1/\tau_1$ (s^{-1})	$1/\tau_2$ (s^{-1})
B-1	2.97×10^8	—
B-2	1.11×10^{12}	4.34×10^8
B-3	3.72×10^8	—
B-4	1.54×10^{12}	9.42×10^8
B-5	8.43×10^8	—
B-6	2.24×10^{11}	3.70×10^8

overlap with the absorption of C_{60}, but that between **B-6** and C_{60} is much less. As the ISC process only occurs in the C_{60} moiety, the ISC rates of the three photosensitizers are in the same time order of magnitude as indicated in Table 2.

$$C_{60}\text{–}{}^1\text{bodipy}^* \rightarrow {}^1C_{60}^*\text{–bodipy} \quad \text{resonance energy transfer (RET)} \tag{1}$$

$${}^1C_{60}^*\text{–bodipy} \rightarrow {}^3C_{60}^*\text{–bodipy} \quad \text{intersystem crossing (ISC)} \tag{2}$$

In order to further confirm the C_{60}-localized triplet state, the spin density surfaces of the lowest T_1 states of the dyads were calculated at the B3LYP and TD-B3LYP levels[13] and shown in Fig. 3. For **B-2**, the spin density is mainly localized on the C_{60} unit, while the bodipy antenna does not contribute to the spin density surface. Similarly, the spin densities of **B-4** and **B-6** are also exclusively localized on the C_{60} moiety. The present calculations are excellently consistent with the femtosecond time-resolved transient absorption spectra.

3.3 Nanosecond transient difference absorption spectra

As the triplet C_{60} monomer, ${}^3C_{60}^*$, has a very long lifetime,[54] the quenching of a triplet dyad by collision with the molecules in solution becomes very important and even dominant in its all feasible decay pathways. Thus, the lifetimes of the triplet dyads are hardly predicted intuitively. In order to study the photochemical characteristics of the lowest triplet state of these three dyads, ${}^3C_{60}^*$–bodipy, the nanosecond time-resolved transient difference absorption spectra were measured and shown in Fig. 4(a–c).

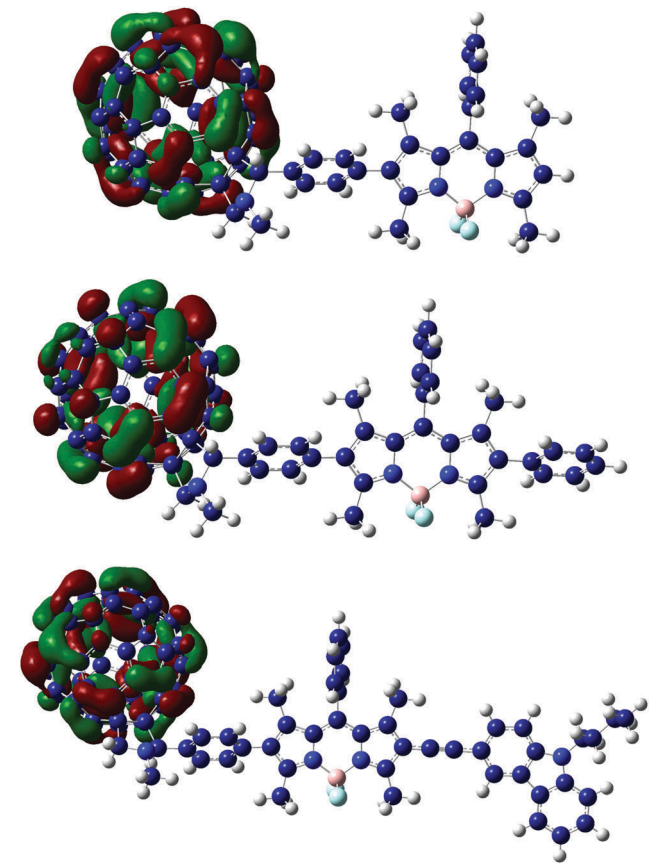

Fig. 3 Spin density surfaces of **B-2**, **B-4**, and **B-6** at the lowest triplet state. Toluene was used as a solvent in the calculations.

For **B-2**, two transient absorptions centered at 370 and 726 nm are observed in Fig. 4(a), and both of them are well known as the characteristic absorptions of the ${}^3C_{60}^*$ unit.[34] An additional experiment was performed to verify the assignment, in which the absorption intensities of both the bands were quenched drastically in the presence of solvated oxygen. A positive band at ~520 nm is observed for **B-2** due to absorption of the bodipy antenna (**B-1** core), while the ground state bleaching of the antenna at 517 nm (negative peak) is not observed for **B-2** yet. Thus, the lowest triplet state T_1 of the dyad seems exclusively localized on the C_{60} unit. This conclusion is consistent with the above prediction of the femtosecond transient absorption spectra and the spin density surface calculations. As shown in Fig. 4(d), the lifetime of the triplet excited state is determined as 35.6 μs in deaerated toluene, while it is reduced to 0.31 μs in aerated toluene. Similar transient absorption spectra were observed for **B-4** in Fig. 4(b) and **B-6** in Fig. 4(c). The lifetimes of the triplet states of **B-4** and **B-6** are determined as 39.8 μs and 33.7 μs, and reduced to 0.29 μs and 0.37 μs in air conditions, respectively. Compared with ${}^3C_{60}^*$ itself, the lifetimes of the dyads reduce by almost a half. The photochemical properties of the dyads and C_{60} itself are summarized in Table 3.

3.4 TTA upconversion spectra

In the fluorescence emission spectra of Fig. 1(b), only two very weak fluorescence emissions at 540 nm and 710 nm were observed in **B-2**. The emissions are assigned as the contributions of the bodipy core and C_{60} unit. When perylene was added in the deaerated solution of **B-2**, a very strong blue-light emission was observed. Fig. 5(a–c) shows the fluorescence emission spectra recorded in the presence of perylene, where the asterisks indicate the scattered excitation laser at 532 nm. The blue emission covers a visible wavelength range from 420 to 540 nm. Photoexcitation of perylene itself in deaerated solution at 532 nm does not exhibit fluorescence in the same experimental conditions. Moreover, such blue emission cannot be observed either in the mixed solution of **B-2** and perylene when solvated oxygen exists. Therefore, the strong blue emission is believed to be produced by TTA-UC of perylene following the triplet–triplet energy transfer (TTET) from ${}^3C_{60}^*$ to perylene, where the dyads act as the triplet photosensitizers and perylene is the triplet acceptor in the mixed solution.

The upconverted fluorescence intensity has a quadratic dependence on the excitation power at low intensities and shifts to a linear dependence at higher power density.[55] Thus, the TTA-UC threshold excitation intensity, I_{th}, is an important parameter, where the incident laser power dependence of the upconverted fluorescence intensity changes from quadratic to linear. When the excitation power density is lower than I_{th}, the quantum yield of TTA-UC, Φ_{UC}, is linearly dependent on the

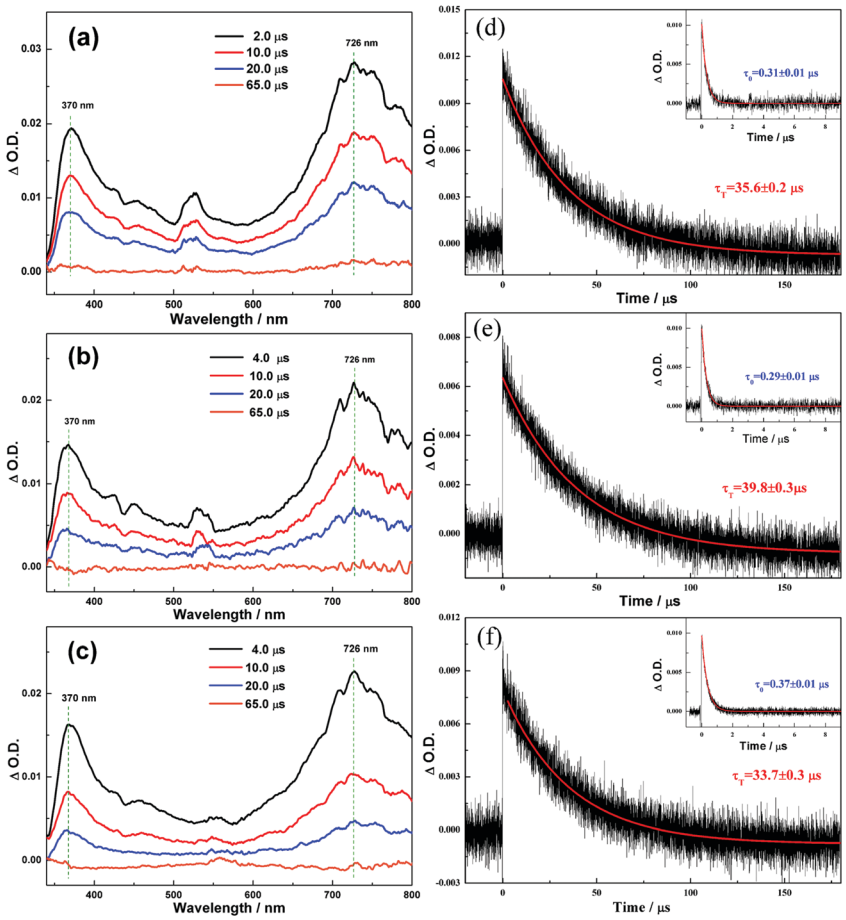

Fig. 4 Nanosecond time-resolved transient difference absorption spectra of **B-2** (a), **B-4** (b), and **B-6** (c), and decay dynamic curves of **B-2** (d), **B-4** (e), and **B-6** (f) at 726 nm (in toluene, $c = 5 \times 10^{-6}$ M, 25 °C) under excitation at 532 nm.

Table 3 Absorption, fluorescence emission wavelengths, and lifetimes of the triplet excited state of the dyads and C_{60} in deaerated (τ_T) and aerated toluene (τ_0)[a]

Compound	λ_{absorp} (nm)	$\lambda_{emission}$ (nm)	τ_T (μs)	τ_0 (μs)
C_{60}	283/336/532	415/439/680	63.6 ± 1.8	0.35 ± 0.04
B-2	518	543	35.6 ± 0.2	0.31 ± 0.01
B-4	532	562	39.8 ± 0.3	0.29 ± 0.01
B-6	557	624	33.7 ± 0.3	0.37 ± 0.01

[a] Excited at 532 nm with 8.6 mJ per pulse, concentration is 5×10^{-6} M, in toluene, 25 °C.

incident laser power. Until it is beyond I_{th}, Φ_{UC} reaches the maximum and the TTA process becomes the dominant deactivation channel for the triplet acceptor.[14,56]

Fig. 6 shows the dependence of the upconverted emission intensity of the dyads on the excitation power density. The slopes close to 2 were observed for **B-2** in the double logarithmic plot when the power density is low. When the power increases, the slope gradually becomes close to 1. From the relationship in Fig. 6, I_{th} is determined as 597 mW cm^{-2} for **B-2**, 589 mW cm^{-2} for **B-4** and 695 mW cm^{-2} for **B-6**, in the present experimental conditions. Therefore, the TTA-UC quantum yields Φ_{UC} of the dyads as the triplet photosensitizer were quantitatively measured with an excitation power density over I_{th}, and the typical value was 790 mW cm^{-2}.

In order to compare the TTET efficiencies between the different dyads and perylene, the quenching rates of the triplet excited state of the photosensitizers were measured, where the concentrations of the dyads were fixed at 5×10^{-6} M. Fig. 7 shows the Stern–Volmer linear relationships. The quenching rate of $^3C_{60}$* by perylene was also measured to compare to those of the dyads. The quenching constants K_{SV} in the Stern–Volmer relationship (3) are determined as 1.88×10^4 M^{-1} for **B-2**, 2.29×10^4 M^{-1} for **B-4** and 1.73×10^4 M^{-1} for **B-6**. The quenching rate constants k_q are 0.53×10^9 M^{-1} s^{-1} for **B-2**, 0.58×10^9 M^{-1} s^{-1} for **B-4** and 0.51×10^9 M^{-1} s^{-1} for **B-6**. The K_{SV} and k_q of $^3C_{60}$* are 14.41×10^4 M^{-1} and 2.26×10^9 M^{-1} s^{-1}, which are much faster than those of the dyads.

$$\frac{\tau_0}{\tau} - 1 = K_{SV} \cdot [\text{perylene}] \quad (3)$$

where τ_0 and τ are the triplet state lifetimes of the photosensitizer in the absence and presence of perylene, respectively.

Using the fluorescence of compound **3** as the standard (Φ_{std} = 2.7% in ACN), the TTA-UC quantum yields, Φ_{UC}, can

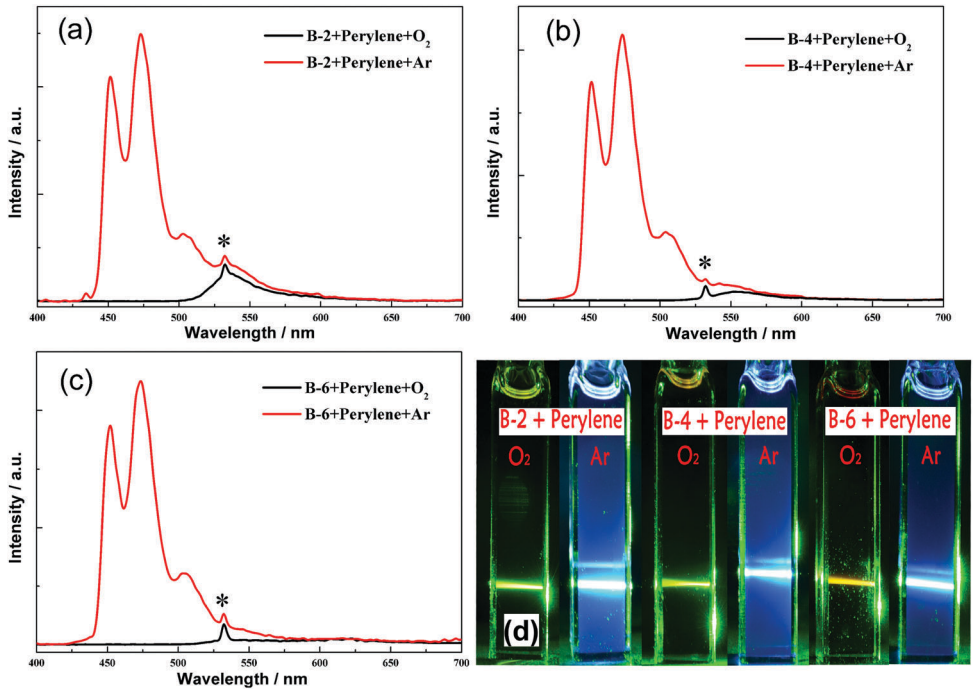

Fig. 5 TTA upconversion spectra of (a) **B-2**, (b) **B-4**, and (c) **B-6** as the triplet photosensitizers (5×10^{-6} M) and perylene (3×10^{-4} M) as the triplet acceptor, (d) photographs of the upconverted fluorescence emissions of these TTA-UC systems in the presence and absence of solvated oxygen, under photoexcitation with a CW laser (at 532 nm with 790 mW cm^{-2}) in toluene, 25 °C.

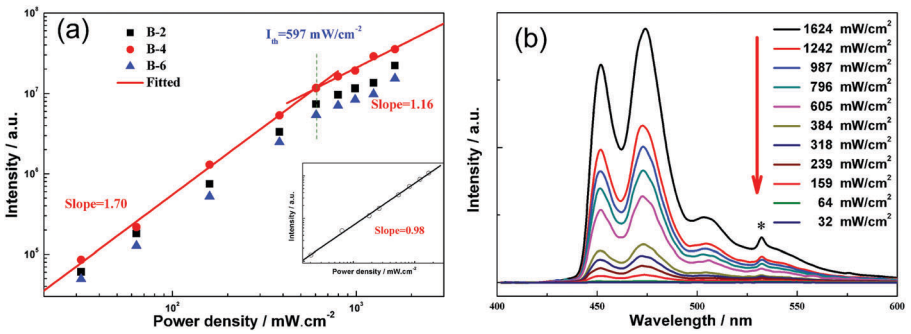

Fig. 6 (a) The double logarithmic plot of integrated upconverted emission dependence on the excitation power density of **B-2**, **B-4**, and **B-6**, where that of the normal fluorescence intensity of **B-1** under excitation at 532 nm is shown in the inserted panel, c[**B-1**] = 5×10^{-6} M. (b) The upconverted emission dependence on the excitation power density of **B-2**, where c[**B-2**] = 5×10^{-6} M, c[perylene] = 3×10^{-4} M, in toluene and excitation is at 532 nm, 25 °C.

be determined with eqn (4),

$$\Phi_{UC} = 2 \cdot \Phi_{std} \cdot \left(\frac{A_{std}}{I_{std}}\right) \cdot \left(\frac{I_{sam}}{A_{sam}}\right) \cdot \left(\frac{\eta_{sam}}{\eta_{std}}\right)^2 \quad (4)$$

where A, I, and η are the absorbance intensity, integrated luminescence intensity, and refractive index of the solvents used for the standard and the samples. In the equation, a factor of 2 is multiplied in order to make the maximum quantum yield be unity.[16] Thus, the Φ_{UC} values for **B-2**, **B-4**, and **B-6** are determined as 5.80%, 7.95%, and 4.99%, and listed in Table 3. The Φ_{UC} values of the three dyads show a consistent trend with the quenching rate constants, K_{SV} or k_q, but do not have a simple proportional relationship. Compared with the reported dyads consisting of bodipy derivatives and C_{60}, *e.g.* carbazole–bodipy–carbazole–C_{60} dyad and bodipy–thiophene–C_{60}, the TTA-UC quantum yields of perylene in the present three systems have been increased about two-fold.

3.5 Theoretical TTA-UC quantum yield

As shown in Scheme 2, there are five steps included in the TTA-UC process to emit fluorescence, intramolecular RET from ^{1}bodipy* to the C_{60} unit in the dyad, ISC from bodipy–$^1C_{60}$* to bodipy–$^3C_{60}$*, TTET from bodipy–$^3C_{60}$* to ^{3}perylene*, TTA of two ^{3}perylene* molecules to produce ^{1}perylene*, and fluorescence emission of ^{1}perylene*. Therefore, the overall TTA-UC quantum yield, Φ_{UC}, can be expressed as eqn (5),

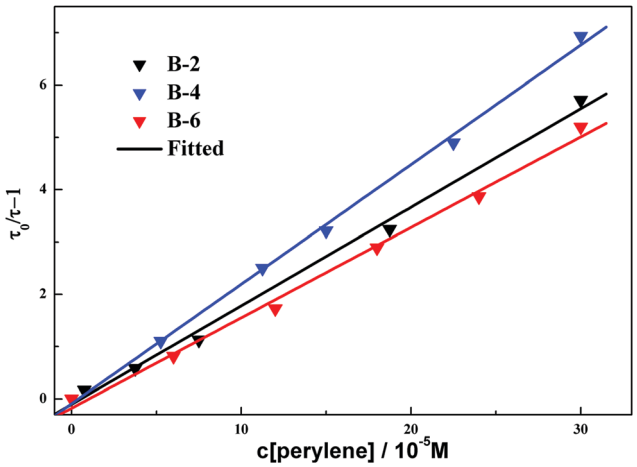

Fig. 7 Stern–Volmer plots for lifetime quenching of the triplet photosensitizers with the concentration of perylene, at 532 nm with 8.6 mJ per pulse power, c[dyad] = 5 × 10^{-6} M, in deaerated toluene, 25 °C.

$$\Phi_{UC} = \Phi_{RET}\cdot\Phi_{ISC}\cdot\Phi_{TTET}\cdot\Phi_{TTA}\cdot\Phi_{F} \quad (5)$$

where Φ_{RET}, Φ_{ISC}, Φ_{TTET}, Φ_{TTA}, and Φ_{F} are the quantum yields of the above processes, respectively.

In the TTA-UC systems of the C_{60}–bodipy dyads and perylene, the concentration of perylene as the energy receptor was the same, and thus the TTA efficiency Φ_{TTA} and the fluorescence yield Φ_{F} of perylene are exactly the same. As discussed above, the lifetimes of the triplet excited state of the three dyads are more than twenty microseconds in deaerated toluene, and the spin density is mainly localized on the C_{60} unit. Thus, all the ISC efficiencies Φ_{ISC} of the C_{60}–bodipy dyads are believed to be close to 1 as well as C_{60} itself. Therefore, the differences of Φ_{UC} among the three TTA-UC systems are mainly coming from the different efficiencies of the RET and TTET processes.

Based on the Jablonski diagram of Scheme 2, the fluorescence quantum yields can be determined by the two equations (6), where Φ_{ad} and Φ_{d} represent the yields in the presence and absence of C_{60}, respectively. The RET efficiency, Φ_{RET}, can be calculated using eqn (7),

$$\Phi_{ad} = \frac{k_{FL}}{k_{NR}+k_{FL}+k_{ET}}, \quad \Phi_{d} = \frac{k_{FL}}{k_{NR}+k_{FL}} \quad (6)$$

$$\Phi_{RET} = \frac{k_{ET}}{k_{NR}+k_{FL}+k_{ET}} = 1-\frac{\Phi_{da}}{\Phi_{d}} \quad (7)$$

where k_{NR} is the nonradiation rate constant, k_{FL} is the fluorescence emission rate constant, and k_{ET} is the rate constant of the intramolecular singlet–singlet RET from the antenna to C_{60}. As the light-harvesting antenna and C_{60} are separated by benzene in the dyads, the interaction between the antenna and C_{60} should be very weak, which is consistent with the fact that no apparent wavelength-shift was observed in the absorption spectra of the dyads from that of the antennas (in Fig. 1). Thus, k_{NR} and k_{FL} are expected to be the same as the values of the antennas themselves.

As shown in Table 1, the fluorescence quantum yield Φ_{d} of the antenna **B-1** is measured to be 82.3%. When C_{60} is connected with **B-1**, the fluorescence is dramatically quenched in the dyad, **B-2**, due to the efficient RET. The fluorescence quantum yield Φ_{ad} of **B-2** is only 0.4%. Thus, the ET efficiency Φ_{RET} is calculated to be 99.5% for **B-2** using eqn (7). Similarly, Φ_{RET} for **B-4** and **B-6** are 99.9% and 99.1%, respectively.

In the presence of perylene, the bimolecular reaction of TTET occurs between it and the triplet dyads. The corresponding efficiency, Φ_{TTET}, can be determined as eqn (8), without taking into account the weak phosphorescence emission.

$$\Phi_{TTET} = \frac{k_{TTET}\cdot[\text{perylene}]}{k_{TTET}\cdot[\text{perylene}]+k_{NR}} = \frac{1/\tau - 1/\tau_{T}}{1/\tau} \quad (8)$$

where k_{NR} is the rate constant of the overall nonradiation process including collision and internal conversion, and k_{TTET} is the quenching rate constant of the triplet photosensitizer by perylene. k_{NR} can be determined as $k_{NR} = 1/\tau_{T}$, and $k_{TTET}\cdot[\text{perylene}]$ is expressed by $(1/\tau - 1/\tau_{T})$, where τ_{T} and τ are the lifetimes of the triplet dyad in the absence and presence of

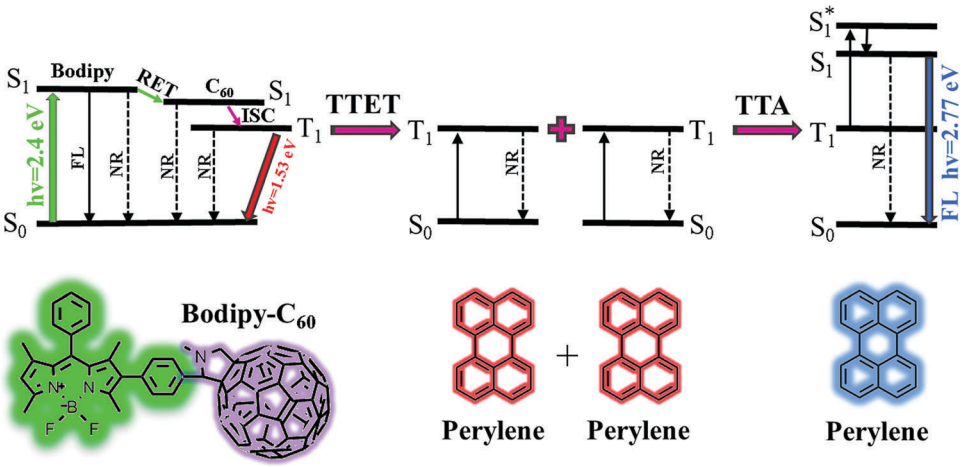

Scheme 2 Jablonski diagram of TTA upconversion of the C_{60}–bodipy derivatives dyads, where ET is the singlet-to-singlet energy transfer, IC is non-radiation, and FL is fluorescence.

Table 4 Lifetimes (τ), Stern–Volmer quenching constants (K_{SV}) and bimolecular quenching rate constants (k_q) of the triplet dyads and C_{60} in the presence of perylene. The experimental TTA upconversion quantum yields (Φ_{UC}) are listed as well[a]

Compound	τ^b (μs)	$K_{SV}{}^c$ ($\times 10^4$ M^{-1})	$k_q{}^c$ ($\times 10^9$ M^{-1} s^{-1})	$\Phi_{UC}{}^d$ (%)
C_{60}	1.4 ± 0.14	14.4 ± 0.6	2.26 ± 0.18	—
B-2	5.3 ± 0.07	1.9 ± 0.1	0.53 ± 0.03	5.80 ± 0.3
B-4	5.0 ± 0.09	2.3 ± 0.1	0.58 ± 0.03	7.95 ± 0.3
B-6	5.4 ± 0.09	1.7 ± 0.1	0.51 ± 0.03	4.99 ± 0.3

[a] Excited at 532 nm, c[photosensitizer] = 5 × 10^{-6} M, toluene, 25 °C. [b] c[perylene] = 3 × 10^{-4} M, in deaerated toluene. [c] In deaerated toluene, 25 °C. [d] Using compound **3** as a standard (Φ_F = 2.7%, in MeCN).

Table 5 Energy transfer efficiencies (Φ_{ET}) and triplet–triplet energy transfer efficiencies (Φ_{TTET}) for the present TTA-UC systems. The experimental TTA-UC quantum yields Φ_{UC} are listed as well

	Φ_{ET}	Φ_{TTET}	$\Phi_{ET}\cdot\Phi_{TTET}$	ε'^a	Φ_{UC} (%)
B-2	0.995	0.851	0.847	0.37	5.80
B-4	0.999	0.874	0.873	0.59	7.95
B-6	0.991	0.839	0.831	0.30	4.99

[a] ε' is the molar extinction coefficient at 532 nm.

perylene, respectively. Using the τ and τ_T values in Tables 3 and 4, the TTET efficiencies between the triplet photosensitizers and perylene are calculated and listed in Table 5.

As mentioned earlier, the differences of Φ_{UC} among the three systems of dyads and perylene mainly come from the different quantum yields of the RET and TTET processes. As shown in Table 5, the Φ_{RET} values are almost the same and very close to unity for the three dyads. Thus, the TTET efficiency becomes the unique potential reason to produce the difference of Φ_{UC}. However, Φ_{TTET} in Table 5 is determined to be 0.851 for **B-2**, 0.874 for **B-4**, and 0.839 for **B-6**. Although the sequence of the Φ_{TTET} value is consistent with that of the experimental Φ_{UC} data, these data do not show a strictly linear relationship between the $\Phi_{RET}\cdot\Phi_{TTET}$ and Φ_{UC} values. It is worth noting that the slope in Fig. 6(a) at the present power density of 790 mW cm^{-2} is beyond 1. This means that the influence of the excitation power still exists to some extent although the power density is over I_{th}. In this case, a slight dependence of Φ_{UC} on the excitation power can be expected. Therefore, more excellent consistence can be found in Table 5 between the $\Phi_{RET}\cdot\Phi_{TTET}\cdot\varepsilon'$ and Φ_{UC} values, where ε' is the molar extinction coefficient at 532 nm.

4. Summary and conclusions

Three triplet photosensitizers of C_{60}–bodipy dyad derivates were designed and synthesized. The strong visible absorption of the photosensitizers is kept as that of the bodipy moiety in a wavelength range from 470 to 600 nm. However, the fluorescence emission is dramatically reduced, indicating that efficient intermolecular RET occurs between the bodipy and C_{60} moieties. According to the high ISC quantum yield of $^1C_{60}$*, the lowest triplet dyads are consequently produced, and the spin density is exclusively located on the C_{60} moiety as suggested by theoretical calculation.

The femtosecond transient difference absorption spectra were recorded to investigate the initial dynamic processes under photoexcitation at 532 nm. By the least square fitting of the decay curves of the dyads, the lifetime of the singlet excited state of the photosensitizer was determined in a picosecond timescale, and the intermolecular RET rates of the dyads were around 10^{12} s^{-1}, while ISC from the S_1 to T_1 state occurs with a rate of $\sim 10^8$ s^{-1}.

Using nanosecond transient difference absorption spectra, the lifetimes of the triplet dyads were determined to be 35.6 μs for **B-2**, 39.8 μs for **B-4**, and 33.7 μs for **B-6** in deaerated toluene. With the presence of perylene as the triplet acceptor, TTET between the triplet dyads and perylene occurs efficiently. The bimolecular quenching rate constants, k_q, were measured to be around 5 × 10^8 M^{-1} s^{-1}.

Following the TTET process, the TTA upconverted fluorescence emission of perylene was clearly observed in the deaerated solution. From the TTA-UC spectra, the upconverted fluorescence quantum yield, Φ_{UC}, was determined to be 5.80% for **B-2**, 7.95% for **B-4**, and 4.99% for **B-6**. These values show a consistent trend with the quenching rate constants, K_{SV} (or k_q), but they do not have a simple proportional relationship.

Based on the fact that the RET and ISC processes of the dyads were very efficient (quantum yields were very close to unity), the differences of Φ_{UC} among the three systems were thought to originate mainly from the different TTET quantum yields. The Φ_{TTET} values were calculated to be 0.851 for **B-2**, 0.874 for **B-4** and 0.839 for **B-6**. The non-linear relationship between the Φ_{TTET} and Φ_{UC} values suggests that the influence of the excitation power still exists to some extent although the power density is already over I_{th}. Thus, the absorption cross-section of the dyads at 532 nm cannot be neglected.

Compared with the reported dyads consisting of bodipy derivatives and C_{60}, the TTA-UC quantum yield of perylene in the present three systems is improved. In addition, the Φ_{UC} value does not increase monotonically with the extension of the π-conjugated structure of the bodipy derivative, indicating that the Forest resonance energy transfer and Dexter TTET do not link monotonically with the extension of the pi-conjugated structure. Thus, there is still a long road for us to find a universal link between structure and characteristics when developing a more efficient triplet photosensitizer in TTA-UC processes. Every dynamic step involved in the TTA-UC system should be carefully taken into account as well as absorption.

Acknowledgements

This work was supported by the National Key Basic Research Foundation (Grant No. 2013CB834602 and 2013CB922202) and the National Natural Science Foundation of China (Grant No. 21373194, 21573210 and 11674355). The quantum chemical calculations in this study were performed on the supercomputing

system in the Supercomputing Center of the University of Science and Technology of China. A few experimental instruments were supported by the Ministry of Science and Technology of China (No. 2012YQ220113) as well.

References

1 J. D. Nguyen, E. M. D'Amato, J. M. Narayanam and C. R. Stephenson, *Nat. Chem.*, 2012, **4**, 854–859.
2 S. Maity, M. Zhu, R. S. Shinabery and N. Zheng, *Angew. Chem., Int. Ed.*, 2012, **51**, 222–226.
3 D. Ravelli, M. Fagnoni and A. Albini, *Chem. Soc. Rev.*, 2013, **42**, 97–113.
4 J. Sun, J. Zhao, H. Guo and W. Wu, *Chem. Commun.*, 2012, **48**, 4169–4171.
5 A. Kamkaew, S. H. Lim, H. B. Lee, L. V. Kiew, L. Y. Chung and K. Burgess, *Chem. Soc. Rev.*, 2013, **42**, 77–88.
6 Y. Cakmak, S. Kolemen, S. Duman, Y. Dede, Y. Dolen, B. Kilic, Z. Kostereli, L. T. Yildirim, A. L. Dogan, D. Guc and E. U. Akkaya, *Angew. Chem., Int. Ed.*, 2011, **50**, 11937–11941.
7 S. Erbas, A. Gorgulu, M. Kocakusakogullari and E. U. Akkaya, *Chem. Commun.*, 2009, 4956–4958.
8 F. Schmitt, J. Freudenreich, N. P. Barry, L. Juillerat-Jeanneret, G. Suss-Fink and B. Therrien, *J. Am. Chem. Soc.*, 2012, **134**, 754–757.
9 Y. Y. Cheng, B. Fückel, R. W. MacQueen, T. Khoury, R. G. C. R.
Clady, T. F. Schulze, N. J. Ekins-Daukes, M. J. Crossley, B. Stannowski, K. Lips and T. W. Schmidt, *Energy Environ. Sci.*, 2012, **5**, 6953–6959.
10 B. C. O'Regan, K. Walley, M. Juozapavicius, A. Anderson, F. Matar, T. Ghaddar, S. M. Zakeeruddin, C. Klein and J. R. Durrant, *J. Am. Chem. Soc.*, 2009, **131**, 3541–3548.
11 Q. Liu, B. Yin, T. Yang, Y. Yang, Z. Shen, P. Yao and F. Li, *J. Am. Chem. Soc.*, 2013, **135**, 5029–5037.
12 Q. Liu, T. Yang, W. Feng and F. Li, *J. Am. Chem. Soc.*, 2012, **134**, 5390–5397.
13 C. Zhang, J. Zhao, S. Wu, Z. Wang, W. Wu, J. Ma, S. Guo and L. Huang, *J. Am. Chem. Soc.*, 2013, **135**, 10566–10578.
14 Y. Y. Cheng, T. Khoury, R. G. Clady, M. J. Tayebjee, N. J. Ekins-Daukes, M. J. Crossley and T. W. Schmidt, *Phys. Chem. Chem. Phys.*, 2010, **12**, 66–71.
15 J. S. Lissau, J. M. Gardner and A. Morandeira, *J. Phys. Chem. C*, 2011, **115**, 23226–23232.
16 T. N. Singh-Rachford and F. N. Castellano, *Coord. Chem. Rev.*, 2010, **254**, 2560–2573.
17 J. Zhao, S. Ji and H. Guo, *RSC Adv.*, 2011, **1**, 937–950.
18 Y. Cheng, J. Yang, Y. Qu and P. Li, *Org. Lett.*, 2011, **14**, 98–101.
19 J. Lalevee, M. Peter, F. Dumur, D. Gigmes, N. Blanchard, M. A. Tehfe, F. Morlet-Savary and J. P. Fouassier, *Chem. – Eur. J.*, 2011, **17**, 15027–15031.
20 W. Wu, X. Wu, J. Zhao and M. Wu, *J. Mater. Chem. C*, 2015, **3**, 2291–2301.
21 C. Ulbricht, B. Beyer, C. Friebe, A. Winter and U. S. Schubert, *Adv. Mater.*, 2009, **21**, 4418–4441.
22 W. Y. Wong and P. D. Harvey, *Macromol. Rapid Commun.*, 2010, **31**, 671–713.
23 V. Fernandez-Moreira, F. L. Thorp-Greenwood and M. P. Coogan, *Chem. Commun.*, 2010, **46**, 186–202.
24 Y. Chi and P. T. Chou, *Chem. Soc. Rev.*, 2010, **39**, 638–655.
25 N. Adarsh, R. R. Avirah and D. Ramaiah, *Org. Lett.*, 2010, **12**, 5720–5723.
26 Q. Zhou, M. Zhou, Y. Wei, X. Zhou, S. Liu, S. Zhang and B. Zhang, *Phys. Chem. Chem. Phys.*, 2017, **19**, 1516–1525.
27 A. E. O'Connor, W. M. Gallagher and A. T. Byrne, *Photochem. Photobiol.*, 2009, **85**, 1053–1074.
28 N. J. Turro, V. Ramamurthy and J. C. Scaiano, *Principles of molecular photochemistry: an introduction*, University science books, CA, USA, 2009.
29 B. Valeur and M. N. Berberan-Santos, *Molecular fluorescence: principles and applications*, John Wiley & Sons, 2012.
30 D. P. Specht, P. A. Martic and S. Farid, *Tetrahedron*, 1982, **38**, 1203–1211.
31 H. W. Kroto, J. R. Heath, S. C. O'Brien, R. F. Curl and R. E. Smalley, *Nature*, 1985, **318**, 162–163.
32 F. Diederich, L. Isaacs and D. Philp, *Chem. Soc. Rev.*, 1994, **23**, 243–255.
33 J. W. Arbogast, A. P. Darmanyan, C. S. Foote, F. N. Diederich, R. Whetten, Y. Rubin, M. M. Alvarez and S. J. Anz, *J. Phys. Chem.*, 1991, **95**, 11–12.
34 R. Ziessel, B. D. Allen, D. B. Rewinska and A. Harriman, *Chem. – Eur. J.*, 2009, **15**, 7382–7393.
35 V. Bandi, F. P. D'Souza, H. B. Gobeze and F. D'Souza, *Chem. Commun.*, 2016, **52**, 579–581.
36 A. N. Amin, M. E. El-Khouly, N. K. Subbaiyan, M. E. Zandler, S. Fukuzumi and F. D'Souza, *Chem. Commun.*, 2012, **48**, 206–208.
37 L. Y. Chiang, P. A. Padmawar, J. E. Rogers-Haley, G. So, T. Canteenwala, S. Thota, L. S. Tan, K. Pritzker, Y. Y. Huang, S. K. Sharma, D. B. Kurup, M. R. Hamblin, B. Wilson and A. Urbas, *J. Mater. Chem.*, 2010, **20**, 5280–5293.
38 T. M. Figueira-Duarte, J. Clifford, V. Amendola, A. Gegout, J. Olivier, F. Cardinali, M. Meneghetti, N. Armaroli and J. F. Nierengarten, *Chem. Commun.*, 2006, 2054–2056.
39 V. Bandi, H. B. Gobeze, V. Lakshmi, M. Ravikanth and F. D'Souza, *J. Phys. Chem. C*, 2015, **119**, 8095–8102.
40 M. Ince, A. Hausmann, M. V. Martinez-Diaz, D. M. Guldi and T. Torres, *Chem. Commun.*, 2012, **48**, 4058–4060.
41 L. Huang, X. Yu, W. Wu and J. Zhao, *Org. Lett.*, 2012, **14**, 2594–2597.
42 Y. Liu and J. Zhao, *Chem. Commun.*, 2012, **48**, 3751–3753.
43 J. Venturini, E. Koudoumas, S. Couris, J. M. Janot, P. Seta, C. Mathis and S. Leach, *J. Mater. Chem.*, 2002, **12**, 2071–2076.
44 D. Takahashi, S. Hirono and K. Toshima, *Chem. Commun.*, 2011, **47**, 11712–11714.
45 M. T. Whited, P. I. Djurovich, S. T. Roberts, A. C. Durrell, C. W. Schlenker, S. E. Bradforth and M. E. Thompson, *J. Am. Chem. Soc.*, 2010, **133**, 88–96.
46 R. Ziessel and A. Harriman, *Chem. Commun.*, 2011, **47**, 611–631.
47 W. Wu, J. Zhao, J. Sun and S. Guo, *J. Org. Chem.*, 2012, **77**, 5305–5312.

48 P. Yang, W. Wu, J. Zhao, D. Huang and X. Yi, *J. Mater. Chem.*, 2012, **22**, 20273–20283.
49 R. Zhang, Y. Yang, S. Yang, V. S. Neti, H. Sepehrpour, P. J. Stang and K. Han, *J. Phys. Chem. C*, 2017, **121**, 14975–14980.
50 Y. P. Wang, S. Zhang, S. M. Sun, K. Liu and B. Zhang, *Chin. J. Chem. Phys.*, 2013, **26**, 651–655.
51 M. Frisch, G. W. Trucks, H. B. Schlegel, G. E. Scuseria, M. A. Robb, J. R. Cheeseman, G. Scalmani, V. Barone, B. Mennucci and G. A. Petersson, *Gaussian 09*, Gaussian, Inc., Wallingford, CT, 2009.
52 L. Huang, X. Cui, B. Therrien and J. Zhao, *Chem. – Eur. J.*, 2013, **19**, 17472–17482.
53 W. Wu, H. Guo, W. Wu, S. Ji and J. Zhao, *J. Org. Chem.*, 2011, **76**, 7056–7064.
54 M. Fraelich and R. Weisman, *J. Phys. Chem.*, 1993, **97**, 11145–11147.
55 A. Monguzzi, J. Mezyk, F. Scotognella, R. Tubino and F. Meinardi, *Phys. Rev. B: Condens. Matter Mater. Phys.*, 2008, **78**, 195112.
56 A. Haefele, J. Blumhoff, R. S. Khnayzer and F. N. Castellano, *J. Phys. Chem. Lett.*, 2012, **3**, 299–303.

